Three-Phase Reactor Model to Simulate the Performance of Pilot-Plant and Industrial Trickle-Bed Reactors Sustaining Hydrotreating Reactions

ARTICLE *in* INDUSTRIAL & ENGINEERING CHEMISTRY RESEARCH · SEPTEMBER 2004

Impact Factor: 2.59 · DOI: 10.1021/ie049642b

5 AUTHORS, INCLUDING:

G. Valavarasu
Hindustan Petroleum Corporation Limited
11 PUBLICATIONS **113** CITATIONS
SEE PROFILE

Krishnaswami Balu
Anna University, Chennai
18 PUBLICATIONS **564** CITATIONS
SEE PROFILE

Three-Phase Reactor Model to Simulate the Performance of Pilot-Plant and Industrial Trickle-Bed Reactors Sustaining Hydrotreating Reactions

M. Bhaskar,*,† G. Valavarasu,† B. Sairam,† K. S. Balaraman,† and K. Balu‡

Research and Development Centre, Chennai Petroleum Corporation Limited, Chennai 600 068, India, and A. C. College of Technology, Anna University, Chennai 600 025, India

A three-phase heterogeneous model was developed to simulate the performance of pilot-plant and industrial trickle-bed reactors applied to the hydrodesulfurization of diesel fractions. The model is based on two-film theory and incorporates mass-transfer phenomena at the gas−liquid and liquid−solid interfaces. The major hydrotreating reactions, namely, hydrodesulfurization, hydrodenitrogenation, hydrodearomatization, saturation of olefins, and hydrocracking, were modeled. Detailed pilot-plant experiments were carried out in a continuous-flow trickle-bed reactor using feedstock and catalyst samples collected from an industrial reactor to determine kinetic parameters and to validate the model under various operating conditions. The reactor temperature was varied from 320 to 360 °C and the liquid hourly space velocity from 1.0 to 2.5 h^{-1} at a constant operating pressure of 4.0 MPa and a H_2/oil ratio of 200 L/L. The three-phase heterogeneous model was solved to estimate kinetic parameters for various hydrotreating reactions using the data generated in pilot-plant experiments. A partial wetting model was proposed to account for incomplete wetting of the catalyst particles in pilot-plant reactors. The model simulations were found to agree well with the experimental data in the range of operating conditions studied. A three-phase nonisothermal heterogeneous model with complete catalyst wetting was applied to simulate the performance of an industrial reactor under various operating conditions using the kinetic parameters estimated from pilot-plant experiments. Temperature profiles in the industrial reactor were generated. The model was found to simulate the performance of the industrial reactor adequately. The model was also applied to study the influence of operating conditions such as reactor temperature and feed rate on product quality.

Introduction

Trickle-bed reactors can be defined as fixed beds of catalyst particles contacted by cocurrent downward flow of gas and liquid phases at low superficial velocities. These reactors assume greater importance among the three-phase gas−liquid−solid reaction systems encountered in industrial practice. Trickle-bed reactors belong to a special case of fixed-bed reactors involving gas and liquid phases and a solid catalyst. Various flow regimes can be encountered in fixed-bed reactors depending upon the superficial mass velocities, fluid properties, and bed characteristics. Specchia et al.[1] and Al-Dahhan et al.[2] have subdivided the flow regimes into low-interaction and high-interaction regimes according to the gas−liquid interactions encountered. The low-interaction regime includes trickle flow, whereas the high-interaction regime includes pulse, wavy, spray, and bubble flow patterns. The trickle-flow regime appears at relatively low gas and liquid velocities. In the trickle-flow regime, the liquid reactant flowing down through the reactor forms a thin film around the solid catalyst. The gas reactant, being the continuous phase, fills the remaining void space of the catalyst bed and flows separately.

Trickle-bed reactors are widely employed in petroleum refineries for hydrotreating, hydrofinishing, hydrodesulfurization, and hydrocracking applications. Prior to industrial application, catalysts are generally evaluated in pilot-plant reactors to generate kinetic data, study the influence of operating conditions, etc. The length of an industrial trickle-bed reactor is normally 10−20 times greater than that of a pilot-plant reactor; therefore, it is not possible to operate pilot-plant and industrial reactors at the same liquid hourly space velocity (LHSV) and superficial mass velocity simultaneously. Generally, experiments are conducted at the industrial reactor space velocity, causing the superficial mass velocity in the pilot-plant reactor to be 10−20 times lower. The lower superficial mass velocities observed in smaller reactors result in lower levels of conversion. The lower liquid velocities encountered in pilot-plant reactors also result in incomplete wetting of the catalyst particles. Moreover, the axial dispersion or backmixing effects become significant in some pilot-plant reactors, whereas they are negligible in the case of industrial reactors. Wall effects and liquid maldistribution are some of the other problems reported to be present in pilot-plant reactors. The difference in the operation of pilot-plant and industrial reactors is presented in Table 1.

Because of these differences, it becomes difficult to correlate data from a pilot-plant with those from an industrial reactor. Mathematical models are generally employed to simulate the performance of the pilot-plant

* To whom correspondence should be addressed. Tel.: +91 (44) 25944389. Fax.: +91 (44) 25941338. E-mail: bhaskarm@cpcl.co.in.

† Chennai Petroleum Corp. Ltd.

‡ Anna University.

10.1021/ie049642b CCC: $27.50
Published on Web 09/16/2004

Table 1. Differences between Pilot-Plant and Industrial Trickle-Bed Reactors

	industrial reactor	pilot-plant reactor
length	10−25 m	0.5−2.0 m
diameter	1−4 m	0.5−4.0 cm
gas velocity	14.8−2200 cm/s	1.48−220 cm/s
liquid velocity	0.8−2.5 cm/s	0.08−0.25 cm/s
wetting	complete	partial
flow regime	trickle/slug flow	trickle
axial dispersion	negligible	significant in some cases
catalyst irrigation	very good	poor
mass transfer	very good	poor
channeling and wall effects	negligible	significant
mode of operation	nonisothermal	isothermal

reactor, scale-up to the industrial scale, and predict the performance of the industrial-scale reactor from the pilot-plant experiments.

Over the years, many investigators have attempted different approaches to model trickle-bed reactors. The reactor models reported in the literature can be broadly categorized as "kinetic" models and "hydrodynamic" models. The kinetic models are generally based on intrinsic rates of reactions and do not account for the influence of hydrodynamics and related phenomena. Currently, these models are used for testing and evaluating catalysts in bench-scale reactors but cannot be used for scale-up purposes as they neglect the effects of hydrodynamics. The hydrodynamic models emphasize the hydrodynamic aspects of the reactor such as external liquid holdup, catalyst wetting, axial dispersion, etc., and generally assume plug flow with first-order kinetics. The hydrodynamic models incorporate an apparent rate constant in place of the intrinsic rate constant to account for the effects of hydrodynamics.

Henry and Gilbert[3] described a pseudohomogeneous plug-flow model using a first-order kinetics. This model assumes that the apparent rate constant is proportional to the external liquid holdup. Iannibello et al.,[4] Tsamatsoulis et al.,[5] and Froment et al.[6] attempted to model the performance of trickle-bed reactors by assuming pseudohomogeneous kinetics. These models have limitations in application as they are based on a prior assumption of the appropriate kinetics and weak underlying theory.

Korsten and Hoffman[7] presented a three-phase heterogeneous model for the hydrodesulfurization of vacuum gas oil in a trickle-bed reactor. This model was based on two-film theory and incorporated mass-transport phenomena at the gas−liquid and liquid−solid interfaces. The chemical reaction rates were described by a Langmuir−Hinshelwood mechanism. The simulation procedure also included correlations to estimate the mass-transfer coefficients, gas solubilities, and properties of oils and gases under process conditions. This model was used to analyze the performance of a pilot-plant trickle-bed reactor, and the model predictions were found to be in good agreement with the experimental results.

Ramesh Kumar et al.[8] discussed axial dispersion and channeling effects in trickle-bed reactors and addressed the problems faced in correlating pilot-plant data with those from industrial reactors. They studied the performance of certain commercial catalysts employed in the hydrodesulfurization of a diesel oil using a nonlinear power-law kinetics. The relative volume activity of the catalyst was calculated from the ratio of the observed rates of reactions. The axial dispersion and channeling effects were assumed to be negligible on the basis of the criterion suggested by Mears[9] and the radial aspect ratio of the internal diameters of the reactor and catalyst particle.

Bhaskar and Balaraman[10] applied the three-phase heterogeneous model suggested by Korsten and Hoffman[7] to simulate the performance of a pilot-plant trickle-bed reactor sustaining hydrodesulfurization reactions. Bhaskar et al.[11] solved a three-phase heterogeneous model and simulated the performance of pilot-plant reactor under various operating conditions. They produced profiles of concentrations and partial pressures along the catalyst bed length. The simulation results were found to agree well with the experimental results.

Chowdhury et al.[12] investigated the desulfurization and hydrogenation of aromatics of diesel in an isothermally operated trickle-bed reactor using commercial bifunctional Ni−Mo/Al_2O_3 catalysts. They developed a mechanistic mathematical model for a two-phase flow reactor, considering both mass transfer and chemical reactions in the reactor.

Although the models reported in the literature were successfully applied to simulate the performance of pilot-plant reactors, little effort was made to scale up to an industrial reactor. The validation data using different reactors and reaction systems are scarce. Moreover, many of the models reported in the literature have not considered all of the important reactions taking place in a hydrotreating unit. In the present work, efforts are made to develop a rigorous mathematical model that can account for all of the major reactions, include a fair amount of complexity, and simulate the performance of both pilot- and industrial-scale trickle-bed reactors and correlate pilot-plant data with those from an industrial reactor.

Experimental Section

Equipment. The experiments were conducted in a continuous trickle-flow reactor unit designed to operate at a maximum temperature of 600 °C and a maximum pressure of 30.0 MPa. The reactor tube was made of stainless steel 316 with an internal diameter of 2.54 cm and a length of 80 cm. The reactor was operated in isothermal mode by independent temperature control of a four-zone electric furnace. A schematic diagram of the unit is shown in Figure 1.

The pilot-plant experiments were carried out using 200 mL of catalyst in a 45 cm bed. The top 30 cm of the reactor was filled with inert Al_2O_3 spheres to ensure a homogeneous flow distribution of the feed streams, to heat the reactants to the required temperature, and to avoid end effects. The bottom 25 cm of the reactor was filled with inert Al_2O_3 spheres to serve as a disengaging section. Prior to experimental runs, the catalyst was dried and presulfided with diesel spiked with dimethyl disulfide in accordance with the standard method.

Materials. A diesel feedstock collected from a diesel hydrodesulfurization unit of Chennai Petroleum Corporation Limited was used in the present study. The feed is a typical blend of straight-run diesel fractions from crude distillation units, FCC cycle oils, and heavy naphtha. It contains 1.11 wt % of sulfur, 120 ppmw of nitrogen, and 37.4 wt % of total aromatics. The properties of the feedstock used in the present work are presented in Table 2. The catalyst samples that are

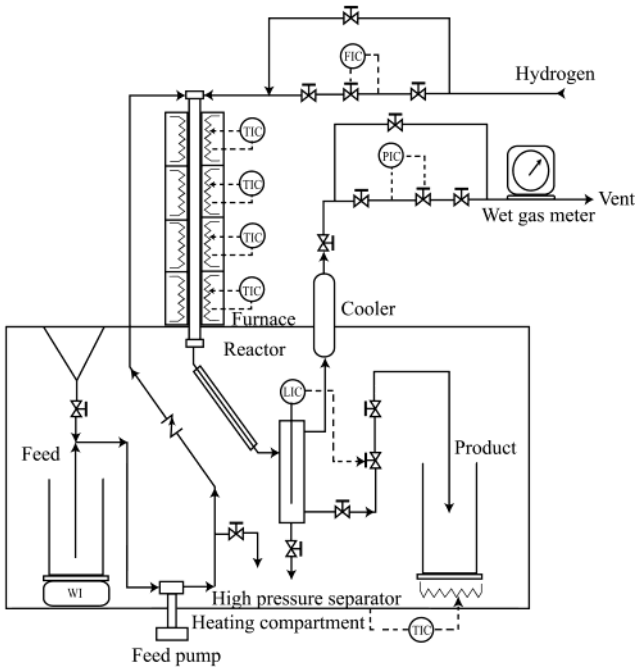

Figure 1. Schematic diagram of the pilot-plant reactor. TIC, temperature indication and control; PIC, pressure indication and control; FIC, flow indication and control; LIC, level indication and control; WI, weight indication.

Table 2. Properties of Diesel Feedstock

property	value
density at 15 °C, g/cm^3	0.8575
viscosity at 40 °C, cSt	3.90
pour point, °C	0
aniline point, °C	71
flash point, °C	118
rams bottom carbon residue, wt %	0.1221
sulfur, wt %	1.11
nitrogen, ppmw	120
olefins, wt %	6.1
total aromatics, wt %	37.40
polyaromatics, wt %	3.50
diaromatics, wt %	10.10
monoaromatics, wt %	23.80
total saturates, wt %	62.60
naphthenes, wt %	19.25
paraffins, wt %	43.35
ASTM D-86 Distillation	
IBP, °C	164
5 vol %, °C	234
10 vol %, °C	247
20 vol %, °C	264
30 vol %, °C	275
50 vol %, °C	294
70 vol %, °C	316
80 vol %, °C	331
90 vol %, °C	350
FBP, °C	370

presently loaded in the industrial unit were used in the experimental work. These catalysts are trilobe extrudates of $NiO-MoO_3/Al_2O_3$ with an average particle diameter of 1.5 mm. The surface area and pore volume of the catalyst samples are 190 m^2/g and 0.43 cm^3/g, respectively.

Experimental Studies. The experiments were carried out at a constant pressure of 4.0 MPa and a constant H_2/oil ratio of 200 L/L. Experiments were performed to study the influence of reactor temperature and liquid hourly space velocity on product quality. The reactor temperature was varied from 320 to 360 °C at different liquid hourly space velocities. The liquid hourly space velocity was varied from 1.0 to 2.5 h^{-1} at different reactor temperatures.

Analytical Methods. The feed and product samples collected from the industrial unit were analyzed to determine their physical properties and measure the contents of sulfur; nitrogen; and olefinic, poly-, di-, and monoaromatic, and naphthenic hydrocarbons. The products collected from the pilot-plant reactor hydrotreated at various operating conditions were also subjected to detailed characterization. The analysis was done as according to ASTM and IP standard test methods.

The sulfur content of the diesel samples was determined using an X-ray fluorescence spectrophotometer (Oxford Lab-X 3500) in accordance with standard ASTM D 4294. Each sample was purged with nitrogen to remove dissolved hydrogen sulfide before analysis. The nitrogen content of the samples was determined using a chemiluminescence method in accordance with standard ASTM D 4629 using an Antek 703C instrument. High-performance liquid chromatography (HPLC) was used to separate and determine the contents of saturates and poly-, di-, and monoaromatics in diesel samples using a Waters 410 instrument in accordance with the IP 360 standard method. The extent of hydrocracking of diesel to lighter products was determined through material balance and gas chromatographic analyses of gas and liquid product samples. The bromine numbers of diesel samples before and after hydrotreating were determined in accordance with standard ASTM D 1159, and the olefin content was estimated from the bromine number.

Model Description

A schematic representation of the trickle-bed reactor model based on two-film theory for the reactions treated in the present work is shown in Figure 2. At steady state, the mass-transfer rate of any component across the gas−liquid interface becomes equal to the mass-transfer rate across the liquid−solid interface. Further, the interfacial mass-transfer rates are equal to the rates of disappearance/formation of various components due to the chemical reactions taking place on the catalyst surface. Hence, model equations can be formulated for all of the reactions according to differential mass balances across the gas−liquid and liquid−solid interfaces.

Reactions Modeled

Under normal operating conditions, hydrotreating catalysts promote several reactions simultaneously. Some of these reactions are desirable, whereas others are not. Hydrodesulfurization, hydrodenitrogenation, olefin saturation, and hydrodearomatization reactions are the important desirable reactions in diesel hydrotreating, whereas hydrocracking and coking are undesirable reactions. Desirable reactions reduce heteroatomic impurities such as sulfur and nitrogen and saturate olefinic compounds.

The reactions discussed in the following subsections were modeled in the present work. These reactions essentially account for all of the major reactions taking place in a hydrotreating unit and assume paramount importance in the design, operation, and optimization of industrial reactors.

Hydrodesulfurization. Sulfur can be present in different structures combined with hydrocarbon mol-

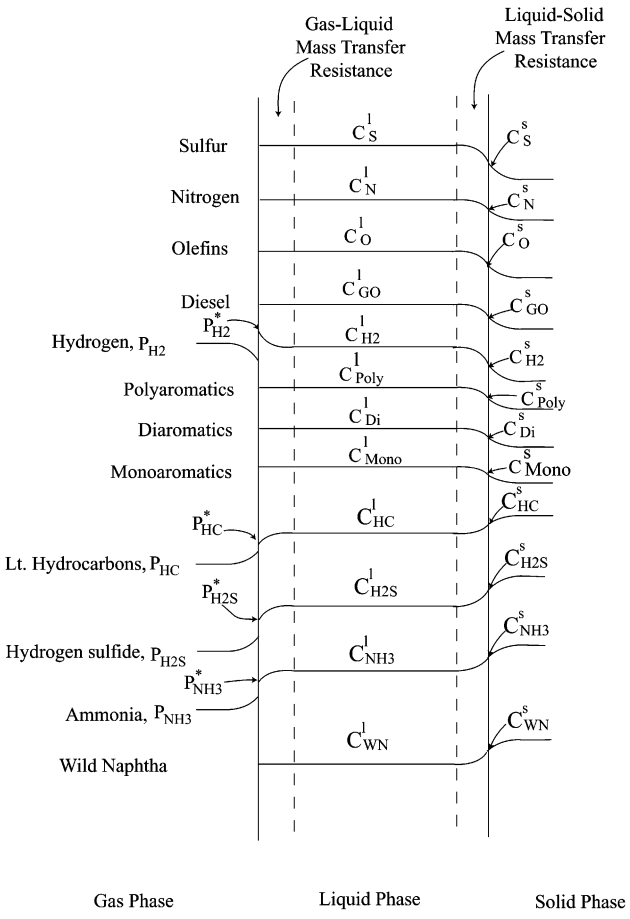

Figure 2. Schematic diagram of the trickle-bed reactor model.

ecules. Sulfur compounds such as thiophenes, benzothiophenes, and alkyl-substituted benzothiophenes are the most common types of sulfur compounds present in diesel fractions. The number of sulfur compounds present in the diesel fraction can be as high as 70 (Ma et al.[13]). Because of the large number of sulfur compounds and problems in their identification and measurement, it is very difficult to model all hydrodesulfurization reactions individually. All of the sulfur compounds are generally grouped as a single lump and considered as a single reaction in studies of the kinetics of desulfurization reactions.[7,11,12]

The following generalized desulfurization reaction was assumed in the present work

$$R{-}S + \frac{3}{2}H_2 \xrightarrow{k_S} R{-}H + H_2S \qquad (1)$$

where R−S is the hydrocarbon structure containing sulfur, H_2 is hydrogen, R−H is the sulfur-free hydrocarbon, and H_2S is hydrogen sulfide. The reaction was assumed to be elementary with the stoichiometric coefficients as shown in eq 1.

Hydrodenitrogenation. Another important reaction that takes place in the hydrotreating of diesel fraction is the removal of nitrogen from the feed. As in the case of desulfurization, all of the nitrogen compounds present in the feed oil are grouped together as a single lump, and the following equation is used for the nitrogen removal reaction

$$R{-}N + 2H_2 \xrightarrow{k_N} R{-}H + NH_3 \qquad (2)$$

where R−N is the hydrocarbon structure containing nitrogen, H_2 is hydrogen, R−H is the nitrogen-free hydrocarbon, and NH_3 is ammonia.

Hydrodearomatization. The aromatic compounds present in the feed oil are grouped into mono-, di-, and polyaromatics. Hydrocarbon molecules that contain one aromatic ring in their structure are grouped as monoaromatics. Hydrocarbons containing two-ring aromatic structures as part of their molecule are grouped as diaromatics. The polyaromatics are defined to contain three or more ring structures.

These aromatic hydrocarbons are hydrogenated to produce naphthenic or lower aromatic hydrocarbons. Each of the aromatic groups undergoes different hydrogenation reactions. In the present work, hydrodearomatization reactions are modeled with the following rate equations

$$\text{polyaromatics} + H_2 \underset{k_{Poly-}}{\overset{k_{Poly}}{\rightleftharpoons}} \text{diaromatics} \qquad (3)$$

$$\text{diaromatics} + 2H_2 \underset{k_{Di-}}{\overset{k_{Di}}{\rightleftharpoons}} \text{monoaromatics} \qquad (4)$$

$$\text{Monoaromatics} + 3H_2 \underset{k_{Mono-}}{\overset{k_{Mono}}{\rightleftharpoons}} \text{naphthenes} \qquad (5)$$

The dearomatization reactions are treated as pseudoreactions with respect to the concentrations of poly-, di-, and monoaromatics as hydrogen is used in excess, as suggested by Girgis and Gates[14] and Wilson and Kriz.[15]

Saturation of Olefins. The olefinic compounds present in the feed oil react with hydrogen to form saturated hydrocarbons. As the feed normally contains cracked streams containing unsaturated hydrocarbons, the hydrogenation of olefins becomes an important reaction. The following equation is assumed to represent olefin saturation

$$R{-}CH{=}CH_2 + H_2 \xrightarrow{k_O} R{-}CH_2{-}CH_3 \qquad (6)$$

Hydrocracking. Acid sites on the Al_2O_3 support promote mild hydrocracking reactions and produce lighter hydrocarbons in gas and liquid products. The cracking reactions are treated using three lumps of diesel, wild naphtha, and light hydrocarbons as described by the reaction

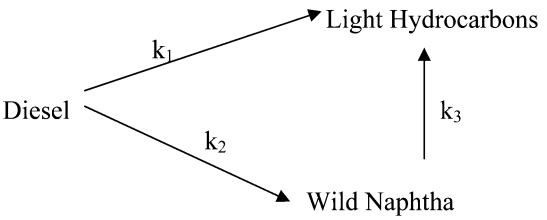

(7)

Model Equations

In the present system of reactions, hydrogen forms the bulk of the gas phase. For the reactions to occur, the hydrogen has to be transferred from the gas phase to the liquid phase and then adsorbed onto the catalyst surface to react with other reactants, namely, sulfur,

nitrogen, aromatics, olefins, and hydrocarbons. The reaction products such as hydrogen sulfide, ammonia, water, and light hydrocarbons will be transported to gas phase as determined by the phase equilibrium at the operating conditions of the reactor. The other reaction products, namely, diesel oil with reduced sulfur, nitrogen, olefins, aromatics, etc., will be transported to the bulk liquid phase. As the vaporization of diesel oil is assumed to be negligible under these conditions, the mass transfer of these components to the gas phase can also be neglected.

Because no reaction occurs in the gas phase, the differential mass balance equation for hydrogen can be written by equating the mass-transfer rate of hydrogen to its pressure gradient in the gas phase as follows

$$\frac{u_G}{RT}\frac{dP_{H_2}}{dz} = -k^l_{H_2}a_p\left(\frac{P_{H_2}}{H_{H_2}} - C^l_{H_2}\right) \tag{8}$$

where u_G is the superficial velocity of the gas, R is the gas constant, T represents the reaction temperature, P_{H_2} is the partial pressure of hydrogen, $C^l_{H_2}$ is the concentration of hydrogen in the liquid phase, and $k^l_{H_2}a_p$ describes the mass transfer between the gas and liquid phases. It is assumed that the gas−liquid equilibrium can be described by Henry's law and that the liquid-phase concentration of hydrogen in equilibrium with the bulk partial pressure is represented by the term P_{H_2}/H_{H_2}, where H_{H_2} is the Henry's coefficient for hydrogen.

On rearranging eq 8, we obtain

$$\frac{dP_{H_2}}{dz} = -\frac{RT}{u_G}k^l_{H_2}a_p\left(\frac{P_{H_2}}{H_{H_2}} - C^l_{H_2}\right) \tag{9}$$

Equation 9 presents a relationship between change in partial pressure of hydrogen in the gas phase and its rate of mass transfer across the gas−liquid interface.

Similarly, we can write equations for the other gas-phase components of the present system of reactions as follows

$$\frac{dP_{H_2S}}{dz} = -\frac{RT}{u_G}k^l_{H_2S}a_p\left(\frac{P_{H_2S}}{H_{H_2S}} - C^l_{H_2S}\right) \tag{10}$$

$$\frac{dP_{NH_3}}{dz} = -\frac{RT}{u_G}k^l_{NH_3}a_p\left(\frac{P_{NH_3}}{H_{NH_3}} - C^l_{NH_3}\right) \tag{11}$$

$$\frac{dP_{HC}}{dz} = -\frac{RT}{u_G}k^l_{HC}a_p\left(\frac{P_{HC}}{H_{HC}} - C^l_{HC}\right) \tag{12}$$

where P_{H_2S}, P_{NH_3}, and P_{HC} are the partial pressures; $k^l_{H_2S}$, $k^l_{NH_3}$, and k^l_{HC} are the mass-transfer coefficients; and $C^l_{H_2S}$, $C^l_{NH_3}$, and C^l_{HC} are the liquid-phase concentrations of hydrogen sulfide, ammonia, and light hydrocarbons, respectively.

Equations 9−12 comprise a system of differential equations that relate the partial pressures of hydrogen, hydrogen sulfide, ammonia, and light hydrocarbons to the mass transfer of the compounds across the gas−liquid interface. They can be solved to obtain partial pressure profiles of the gaseous compounds along the length of the catalyst bed if the liquid-phase concentrations of these components are known.

The differential mass balance equation for the liquid-phase concentration of hydrogen in the reactive zone can be written by equating the concentration gradient to the mass transfer of hydrogen across the gas−liquid and liquid−solid interfaces as follows

$$\frac{dC^l_{H_2}}{dz} = \frac{1}{u_L}\left[k^l_{H_2}a_p\left(\frac{P_{H_2}}{H_{H_2}} - C^l_{H_2}\right) + k^s_{H_2}a_s(C^l_{H_2} - C^s_{H_2})\right] \tag{13}$$

where u_L is the superficial velocity of the liquid, $k^s_{H_2}a_s$ describes the mass transfer across the liquid−solid interface, and $C^s_{H_2}$ is the concentration of hydrogen on the catalyst surface.

Similarly, the mass balance equations for the other gaseous compounds can be written as follows

$$\frac{dC^l_{H_2S}}{dz} = \frac{1}{u_L}\left[k^l_{H_2S}a_p\left(\frac{P_{H_2S}}{H_{H_2S}} - C^l_{H_2S}\right) - k^s_{H_2S}a_s(C^l_{H_2S} - C^s_{H_2S})\right] \tag{14}$$

$$\frac{dC^l_{NH_3}}{dz} = \frac{1}{u_L}\left[k^l_{NH_3}a_p\left(\frac{P_{NH_3}}{H_{NH_3}} - C^l_{NH_3}\right) - k^s_{NH_3}a_s(C^l_{NH_3} - C^s_{NH_3})\right] \tag{15}$$

$$\frac{dC^l_{HC}}{dz} = \frac{1}{u_L}\left[k^l_{HC}a_p\left(\frac{P_{HC}}{H_{HC}} - C^l_{HC}\right) - k^s_{HC}a_s(C^l_{HC} - C^s_{HC})\right] \tag{16}$$

where $k^s_{H_2S}a_s$, $k^s_{NH_3}a_s$, and $k^s_{HC}a_s$ describe the mass transfer across the liquid−solid interface and $C^s_{H_2S}$, $C^s_{NH_3}$, and C^s_{HC} are the surface concentrations of hydrogen sulfide, ammonia, and light hydrocarbons, respectively.

Because the vaporization of diesel oil is negligible under hydrodesulfurization conditions, the organic sulfur, nitrogen, olefins, and aromatics (poly-, di-, and mono-) can be assumed to be nonvolatile. The mass balance equations for these components can be written by equating their liquid-phase concentration gradients to their mass transfer between the liquid phase and the catalyst surface. The mass balance equation for the concentration of organic sulfur in the liquid phase can be written as

$$\frac{dC^l_S}{dz} = -\frac{1}{u_L}k^s_S a_s(C^l_S - C^s_S) \tag{17}$$

where C^l_S and C^s_S are the concentrations of sulfur compounds in the liquid phase and on the catalyst surface, respectively, and $k^s_S a_s$ describes the mass transfer of sulfur compound across the liquid−solid interface.

The mass balance equations for the concentrations of the other components in the liquid phase can be written as

$$\frac{dC_N^l}{dz} = -\frac{1}{u_L}k_N^s a_s(C_N^l - C_N^s) \quad (18)$$

$$\frac{dC_O^l}{dz} = -\frac{1}{u_L}k_O^s a_s(C_O^l - C_O^s) \quad (19)$$

$$\frac{dC_{GO}^l}{dz} = -\frac{1}{u_L}k_{GO}^s a_s(C_{GO}^l - C_{GO}^s) \quad (20)$$

$$\frac{dC_{WN}^l}{dz} = -\frac{1}{u_L}k_{WN}^s a_s(C_{WN}^l - C_{WN}^s) \quad (21)$$

$$\frac{dC_{HC}^l}{dz} = -\frac{1}{u_L}k_{HC}^s a_s(C_{HC}^l - C_{HC}^s) \quad (22)$$

$$\frac{dC_{Poly}^l}{dz} = -\frac{1}{u_L}k_{Poly}^s a_s(C_{Poly}^l - C_{Poly}^s) \quad (23)$$

$$\frac{dC_{Di}^l}{dz} = -\frac{1}{u_L}k_{Di}^s a_s(C_{Di}^l - C_{Di}^s) \quad (24)$$

$$\frac{dC_{Mono}^l}{dz} = -\frac{1}{u_L}k_{Mono}^s a_s(C_{Mono}^l - C_{Mono}^s) \quad (25)$$

$$\frac{dC_{Naph}^l}{dz} = \frac{1}{u_L}k_{Naph}^s a_s(C_{Naph}^l - C_{Naph}^s) = -\frac{dC_{Mono}^l}{dz} = \frac{1}{u_L}k_{Mono}^s a_s(C_{Mono}^l - C_{Mono}^s) \quad (26)$$

where C_N^l and C_N^s are the concentrations of nitrogen in the liquid phase and on the catalyst surface, respectively, and C_O^l and C_O^s represent the corresponding concentrations of olefinic hydrocarbons. As discussed earlier, a three-lump kinetic scheme was assumed to represent the hydrocracking of diesel oil, GO, into wild naphtha, WN, and light hydrocarbons, HC. C_{GO}^l, C_{GO}^s, C_{WN}^l, C_{WN}^s, C_{HC}^l, and C_{HC}^s represent the concentrations of diesel oil, wild naphtha, and light hydrocarbons in the liquid phase and on the catalyst surface. Similarly, C_{Poly}^l, C_{Poly}^s, C_{Di}^l, C_{Di}^s, C_{Mono}^l, C_{Mono}^s, C_{Naph}^l, and C_{Naph}^s are the concentrations of poly-, di-, and monoaromatics and naphthenes in the liquid phase and on the catalyst surface. The factors $k_N^s a_s$, $k_O^s a_s$, $k_{GO}^s a_s$, $k_{WN}^s a_s$, $k_{HC}^s a_s$, $k_{Poly}^s a_s$, $k_{Di}^s a_s$, $k_{Mono}^s a_s$, and $k_{Naph}^s a_s$ describe the mass transfer of nitrogen, olefins, diesel oil, wild naphtha, light hydrocarbons, aromatics (poly-, di-, and mono-), and naphthenes, respectively, across the liquid−solid interface.

The concentrations of the various compounds in the liquid phase can be estimated from their weight fractions in the liquid and molecular weights and the density of the liquid.

Equations 17−26 can be integrated along the length of the catalyst bed to obtain concentration profiles of sulfur, nitogen, olefins, diesel, wild naphtha, light hydrocarbons, aromatics (poly-, di-, and mono-), and naphthenes in the reactor provided that their concentrations on the catalyst surface are known. The concentrations of these components on the catalyst surface change as the reactions proceed along the length of the catalyst bed.

The compounds transferred across the liquid−solid interface are consumed or produced through the chemical reactions. By equating the liquid−solid interfacial mass transfer of these compounds with their reaction rates, we obtain following equations

$$k_{H_2}^s a_s(C_{H_2}^l - C_{H_2}^s) = \rho_B \xi \eta\left(r_S + \frac{3}{2}r_N + r_{Poly} + 2r_{Di} + 3r_{Mono} + r_{GO} + r_{WN} + r_{HC} + r_O\right) \quad (27)$$

$$k_S^s a_s(C_S^l - C_S^s) = \rho_B \xi \eta r_S \quad (28)$$

$$k_{H_2S}^s a_s(C_{H_2S}^l - C_{H_2S}^s) = -\rho_B \xi \eta r_S \quad (29)$$

$$k_N^s a_s(C_N^l - C_N^s) = \rho_B \xi \eta r_N \quad (30)$$

$$k_{NH_3}^s a_s(C_{NH_3}^l - C_{NH_3}^s) = -\frac{3}{2}\rho_B \xi \eta r_N \quad (31)$$

$$k_O^s a_s(C_O^l - C_O^s) = \rho_B \xi \eta r_O \quad (32)$$

$$k_{H_2O}^s a_s(C_{H_2O}^l - C_{H_2O}^s) = -\rho_B \xi \eta r_O \quad (33)$$

$$k_{GO}^s a_s(C_{GO}^l - C_{GO}^s) = \rho_B \xi \eta r_{GO} \quad (34)$$

$$k_{WN}^s a_s(C_{WN}^l - C_{WN}^s) = -\rho_B \xi \eta r_{WN} \quad (35)$$

$$k_{HC}^s a_s(C_{HC}^l - C_{HC}^s) = -\rho_B \xi \eta r_{HC} \quad (36)$$

$$k_{Poly}^s a_s(C_{Poly}^l - C_{Poly}^s) = \rho_B \xi \eta r_{Poly} \quad (37)$$

$$k_{Di}^s a_s(C_{Di}^l - C_{Di}^s) = \rho_B \xi \eta r_{Di} \quad (38)$$

$$k_{Mono}^s a_s(C_{Mono}^l - C_{Mono}^s) = \rho_B \xi \eta r_{Mono} \quad (39)$$

$$k_{Naph}^s a_s(C_{Naph}^l - C_{Naph}^s) = \rho_B \xi \eta r_{Naph} \quad (40)$$

where ρ_B is the bulk density of the catalyst pellets in the bed; η represents the catalyst effectiveness factor; and r_S, r_N, r_O, r_{GO}, r_{WN}, r_{HC}, r_{Poly}, r_{Di}, r_{Mono}, and r_{Naph} represent the intrinsic rates of reaction per unit catalyst mass of sulfur, nitrogen, olefins, diesel oil, wild naphtha, light hydrocarbons, aromatics (poly-, di-, and mono-), and naphthenes, respectively. ξ represents the fraction of the catalyst bed diluted by inerts, defined as

$$\xi = \frac{V_c}{V_c + V_i} \quad (41)$$

where V_c is the volume of active catalyst and V_i is the volume of inert particles. Equations 17−26 are the first-order differential equations representing the concentration profiles of various reactants and products in the liquid phase. Equations 27−40 are the algebraic equations relating the mass transfer across the liquid−solid interface to the reaction rates of various compounds.

Heat Balance. The hydrotreating reactions are exothermic. Because the industrial reactor is operated under nonisothermal conditions, the reactor temperature increases along the length of the reactor. We can

write a differential heat balance equation for the industrial reactor to account for nonisothermal behavior as follows by neglecting the heat-transfer resistance between the liquid and the catalyst surface

$$u_L\rho C_p\frac{dT_R}{dz} = r_S\xi\eta(-\Delta H_S) + r_N\xi\eta(-\Delta H_N) + r_O\xi\eta(-\Delta H_O) + r_{GO}\xi\eta(-\Delta H_{GO}) + r_{Poly}\xi\eta(-\Delta H_{Poly}) + r_{Di}\xi\eta(-\Delta H_{Di}) + r_{Mono}\xi\eta(-\Delta H_{Mono}) \quad (42)$$

where C_p is the specific heat of the feed; T_R is the reactor temperature; and $-\Delta H_S$, $-\Delta H_N$, $-\Delta H_O$, $-\Delta H_{GO}$, $-\Delta H_{Poly}$, $-\Delta H_{Di}$, and $-\Delta H_{Mono}$ are the heats of reaction of hydrodesulfurization, hydrodenitrogenation, olefin saturation, mild hydrocracking of diesel oil, and hydrogenation of poly-, di-, and monoaromatics, respectively.

Of the reactions considered in the present work, hydrodesulfurization and olefin saturation are predominant in terms of heats of reaction. The heat of reaction of dearomatization also assumes significance. The heats of reaction of other reactions can be neglected considering the concentrations of their reactants in the feed and their negligible values. Then, eq 41 can be written as

$$\frac{dT_R}{dz} = \frac{1}{u_L\rho C_p}[r_S\xi\eta(-\Delta H_S) + r_O\xi\eta(-\Delta H_O) + r_{Poly}\xi\eta(-\Delta H_{Poly}) + r_{Di}\xi\eta(-\Delta H_{Di}) + r_{Mono}\xi\eta(-\Delta H_{Mono})] \quad (43)$$

Equation 42 can be integrated along the length of the catalyst bed to obtain temperature profiles in the reactor if the heats of reactions are known or can be determined experimentally. It can be assumed that the heats of reaction do not change with temperature.

Reaction Kinetics. If the reaction rates are known, the above system of equations can be solved simultaneously to obtain the concentrations of the various components in the liquid phase along the length of the catalyst bed and at the outlet.

The following Langmuir−Hinshelwood-type rate equation is used to describe hydrodesulfurization reaction

$$r_S = k_{app,S}\frac{(C_S^s)^{m_1}(C_{H_2}^s)^{m_2}}{(1 + k_{ad}C_{H_2S}^s)^2} \quad (44)$$

where r_S is the rate of reaction per unit mass of the catalyst; C_S^s, $C_{H_2}^s$, and $C_{H_2S}^s$ are the concentrations of sulfur, hydrogen, and hydrogen sulfide, respectively, on the catalyst surface; m_1 and m_2 represent the orders of reaction for sulfur and hydrogen, respectively; $k_{app,S}$ is the apparent rate constant for the hydrodesulfurization reaction; and k_{ad} represents the adsorption equilibrium constant for hydrogen sulfide.

Hydrodesulfurization reactions are known to be irreversible under normal operating conditions.[14] Further, it is also assumed that the concentrations of sulfur and hydrogen have a positive effect on the rate of reaction, whereas the hydrogen sulfide adsorbed on the catalyst surface inhibits the rate of reaction.

The hydrodenitrogenation reaction is also assumed to be irreversible under normal operating conditions. The concentration of hydrogen on the catalyst surface is much higher than the concentration of nitrogen as hydrogen is used as an excess reactant. The following pseudo-first-order kinetics with respect to the concentration of nitrogen was assumed for the hydrodenitrogenation reaction

$$r_N = k_{app,N}C_N^s \quad (45)$$

where $k_{app,N}$ is the apparent rate constant for the hydrodenitrogenation reaction and C_N^s represents the concentration of nitrogen on the catalyst surface.

Similarly, the olefin saturation reaction is also assumed to be pseudo-first-order with respect to the concentration of olefins, as given by the following rate equation

$$r_O = k_{app,O}C_O^s \quad (46)$$

where $k_{app,O}$ is the apparent rate constant for olefin saturation reaction and C_O^s represents the concentration of olefins on the catalyst surface.

As presented in eq 7, mild hydrocracking reactions were treated using a three-lump model consisting of diesel oil, wild naphtha, and light hydrocarbons. The reactions were assumed to follow pseudo-first-order kinetics as follows

$$r_{GO} = (k_1 + k_2)C_{GO}^s \quad (47)$$

$$r_{WN} = -k_2C_{GO}^s + k_3C_{WN}^s \quad (48)$$

$$r_{HC} = -k_1C_{GO}^s - k_3C_{WN}^s \quad (49)$$

where k_1, k_2, and k_3 are apparent rate constants and C_{GO}^s and C_{WN}^s are the surface concentrations of diesel oil and wild naphtha, respectively.

The following rate equations were used to describe the hydrogenation of aromatics

$$r_{Poly} = k_{Poly}^*P_{H_2}{}^{n_1}C_{Poly}^s - k_{Poly-}C_{Di}^s \quad (50)$$

$$r_{Di} = k_{Di}^*P_{H_2}{}^{n_2}C_{Di}^s - k_{Di-}C_{Mono}^s \quad (51)$$

$$r_{Mono} = k_{Mono}^*P_{H_2}{}^{n_3}C_{Mono}^s - k_{Mono-}C_{Naph}^s \quad (52)$$

$$r_{Naph} = -r_{Mono} = -k_{Mono}^*C_{Mono}^sP_{H_2}{}^{n_3} + k_{Mono-}C_{Naph}^s \quad (53)$$

where k_{Poly}^*, k_{Di}^*, k_{Mono}^*, and k_{Naph}^* and k_{Poly-}, k_{Di-}, k_{Mono-}, and k_{Naph-} are the forward and backward rate constants; P_{H_2} is the partial pressure of hydrogen, and n_1, n_2, and n_3 are the exponents of hydrogen.

Because $P_{H_2}{}^{n_1}$, $P_{H_2}{}^{n_2}$, and $P_{H_2}{}^{n_3}$ remain constant when the reaction pressure is held constant, eqs 50−53 reduce to

$$r_{Poly} = k_{Poly}C_{Poly}^s - k_{Poly-}C_{Di}^s \quad (54)$$

$$r_{Di} = k_{Di}C_{Di}^s - k_{Di-}C_{Mono}^s \quad (55)$$

$$r_{Mono} = k_{Mono}C_{Mono}^s - k_{Mono-}C_{Naph}^s \quad (56)$$

where

$$k_{\text{Poly}} = k^*_{\text{Poly}} P_{\text{H}_2}{}^{n_1} \tag{57}$$

$$k_{\text{Di}} = k^*_{\text{Di}} P_{\text{H}_2}{}^{n_2} \tag{58}$$

$$k_{\text{Mono}} = k^*_{\text{Mono}} P_{\text{H}_2}{}^{n_3} \tag{59}$$

Now, k_{Poly}, k_{Di}, and k_{Mono} are the forward rate constants for the hydrogenation of aromatics reactions. To determine the rate constants for the backward reactions, dynamic equilibrium constants were defined as follows

$$K_{\text{Poly}} = \frac{k_{\text{Poly}}}{k_{\text{Poly}-}} \tag{60}$$

$$K_{\text{Di}} = \frac{k_{\text{Di}}}{k_{\text{Di}-}} \tag{61}$$

$$K_{\text{Mono}} = \frac{k_{\text{Mono}}}{k_{\text{Mono}-}} \tag{62}$$

The equilibrium constants at a reference temperature are taken from the data reported by Chowdhury et al.[12] The van't Hoff correlation, as defined below, was used to determine dynamic equilibrium constants at different temperatures

$$\frac{\mathrm{d}(\ln K_{\text{Poly/Di/Mono}})}{\mathrm{d}T} = \frac{\Delta H_{\text{Poly/Di/Mono}}}{RT^2} \tag{63}$$

where $\Delta H_{\text{Poly/Di/Mono}}$ represents the heats of the various hydrogenation of aromatics reactions. The heat of reaction for the dearomatization reaction is assumed to be 67 kJ/mol of hydrogen reacted.[12] The van't Hoff correlation was used to estimate equilibrium constants for dearomatization reactions at various reactor temperatures. The Arrhenius equation was used to account for the temperature dependency of the rate constants for the reactions modeled in the present work.

Results and Discussion

The three-phase heterogeneous reactor model developed in the present work was applied to generate kinetic parameters for various reactions and simulate the performance of a pilot-plant trickle-bed reactor. The experimental data on the performance of two different catalysts (catalysts A and B) were used to validate the model under various operating conditions.

The reactor model comprises a set of first-order differential equations and algebraic equations. These equations are to be solved simultaneously to obtain concentration profiles of various reactants and products in the liquid and gas phases and at the reactor outlet. Because the system of equations cannot be solved analytically, numerical techniques were used. The properties of the gases and liquids, including solubilities, diffusivities, and mass-transfer coefficients, were estimated using the correlations reported in the literature.[7,11]

The orders of the desulfurization reaction with respect to sulfur and hydrogen, m_1 and m_2 in eq 43, are assumed to be 1.0 and 0.45, respectively, in accordance with the results obtained by Korsten and Hoffmann[7] in an investigation of the hydrodesulfurization of vacuum gas oil in a pilot-plant trickle-bed reactor. The adsorption equilibrium constant for hydrogen sulfide is assumed to be 50 000 cm^3/mol as reported by Chowdhury et al.[12] and to remain constant with varying reactor temperature.

Parameter Estimation. The kinetic parameters for the reactions considered in the present work were estimated from the experimental data applying the three-phase trickle-bed reactor model presented in this work. In the case of parameter estimation, the model becomes a boundary-value problem as the concentration of various components, namely, sulfur, nitrogen, olefins, diesel oil, wild naphtha, light hydrocarbons, aromatics (poly-, di-, and mono-), and naphthenes at the reactor inlet and exit are known. Kinetic parameters that agree with the experimental data are to be determined. Because the pilot-plant reactor is operated in isothermal mode, the reactor temperature can be assumed to be constant along the length of the catalyst bed, and hence, the differential equation concerning heat balance can be neglected.

A numerical technique known as the shooting technique was adopted to solve the boundary-value problem to determine the kinetic parameters. The Runge−Kutta fourth-order numerical technique was used to integrate the differential equations along the length of the catalyst bed. The Newton−Raphson technique was used to solve the nonlinear algebraic equations concerning the surface concentrations of various components.

Partial Wetting. The solution of the pilot-plant reactor model to estimate the kinetic parameters showed that the apparent rate constant for the hydrodesulfurization reaction, $k_{\text{app,S}}$, increases with liquid hourly space velocity. This effect can be attributed to catalyst wetting efficiency, defined as the ratio of the apparent rate constant, k_{app}, to the intrinsic rate constant k_{in}. Similar observations were reported by Korsten and Hoffmann.[7] The wetting efficiency of the pilot-plant reactor was reported to be in the range of 0.12−0.6.[16] The wetting efficiency of industrial reactors can be expected to be 0.7−1.0. The wetting efficiency is a function of the initial liquid distribution, the geometry of the packing of the catalyst, and the liquid mass velocities in the reactor. A number of correlations have been reported in the literature for the evaluation of wetting efficiency, and the estimated values were found to scatter in a wide range.[7]

In the present work, the partial wetting model suggested by Satterfield[16] was used to correlate the apparent rate constant, $k_{\text{app,S}}$, with the superficial liquid mass velocity, G_{L} (kg/m^2·s), defined as

$$\frac{1}{k_{\text{app}}} - \frac{1}{k_{\text{in}}} = \frac{A}{G_{\text{L}}{}^B} \tag{64}$$

The rate constants of different hydrotreating reactions for catalysts A and B are reported in Table 3.

Simulation of Pilot-Plant Reactor. The three-phase isothermal reactor model developed in the present work was applied to analyze and simulate the performance of a pilot-plant reactor. The model solution for the pilot-plant reactor becomes an intial-value problem as the concentrations of reactants and products are known at the reactor inlet. The model was solved with the rate constants estimated from pilot-plant studies as discussed in the Parameter Estimation section.

The variation of the sulfur contents in the liquid phase and on the catalyst surface along the length of

Table 3. Rate Constants of Hydrotreating Reactions for Catalysts A and B

	catalyst A		catalyst B	
reaction	expression	k_{in} at 340 °C	expression	k_{in} at 340 °C
$R-S + \frac{3}{2}H_2 \xrightarrow{k_S} R-H + H_2S$	$1.07 \times 10^5 \exp(-13736.6/RT)$	1.36	$6.56 \times 10^4 \exp(-13053.1/RT)$	1.46
$R-N + 2H_2 \xrightarrow{k_N} R-H + NH_3$	$17.67 \exp(-11177.0/RT)$	1.8×10^{-3}	$33.4 \exp(-11811.4/RT)$	2.0×10^{-3}
$R-CH{=}CH_2 + H_2 \xrightarrow{k_{US}} R-CH_2-CH_3$	$0.3749 \exp(-6861.8/RT)$	1.3×10^{-3}	$0.2938 \exp(-6499.2/RT)$	1.4×10^{-3}
$\text{diesel} \xrightarrow{k_1} \text{wild naphtha}$	$1.08 \times 10^{-3} \exp(-4943.2/RT)$	1.87×10^{-5}	$7.78 \times 10^{-4} \exp(-4409.5/RT)$	2.08×10^{-5}
$\text{diesel} \xrightarrow{k_2} \text{light hydrocarbons}$	$3.0 \times 10^{-7} \exp(-4157.2/RT)$	9.88×10^{-9}	$3.4 \times 10^{-7} \exp(-4162.3/RT)$	1.11×10^{-8}
$\text{wild naphtha} \xrightarrow{k_3} \text{light hydrocarbons}$	$1.37 \exp(-9832.6/RT)$	4.28×10^{-4}	$1.21 \exp(-9535.8/RT)$	4.82×10^{-4}
$\text{polyaromatics} + H_2 \xrightleftharpoons{K_{Poly}} \text{diaromatics}$	$2.22 \times 10^8 \exp(-29425.5/RT)$	7.17×10^{-3}	$3.95 \times 10^8 \exp(-30011.6/RT)$	7.89×10^{-3}
$\text{diaromatics} + 2H_2 \xrightleftharpoons{K_{Di}} \text{monoaromatics}$	$1.49 \times 10^6 \exp(-24351.1/RT)$	3.1×10^{-3}	$1.14 \times 10^6 \exp(-23894.3/RT)$	3.45×10^{-3}
$\text{monoaromatics} + 3H_2 \xrightleftharpoons{K_{Mono}} \text{naphthene}$	$6.36 \times 10^5 \exp(-24238.5/RT)$	1.45×10^{-3}	$8.93 \times 10^5 \exp(-24534.6/RT)$	1.6×10^{-3}

the catalyst bed is presented in Figure 3. The concentration profile was generated at a reactor temperature of 320 °C, a pressure of 4.0 MPa, a liquid hourly space velocity of 2.0 h^{-1}, and a H_2/oil ratio of 200 L/L over catalyst A. The simulated concentrations of sulfur on the catalyst surface and in the liquid along the catalyst bed length are shown in Figure 3. The variation of the hydrogen and hydrogen sulfide concentrations on the catalyst surface and in the liquid and the partial pressures in the gaseous phase along the catalyst bed length are shown in Figures 4 and 5.

The simulation results were compared with experimental measurements for hydrodesulfurization, and the results are reported in Tables 4 and 5. As can be seen from the data, the model was found to simulate the performance of the pilot-plant trickle-bed reactor very well in the range of operating conditions studied. The deviation between simulated results and experimental measurements was in the range from −9.72% to +7.05%, in both positive and negative directions. Deviations in this range are acceptable considering the errors associated with conducting pilot-plant experiments and analyzing product samples.

The simulation results for hydrodesulfurization are also compared with experimental data in Figures 6−9 for different catalysts. The lines show the simulation results, and the points represent experimental measurements of sulfur at different operating conditions. As can be seen from Figures 6−9, the partial wetting model was found to represent the experimental data closely. The experimental measurements represented by the points are close to simulated lines. In fact, the simulated lines appear to be the best fit of the experimental points in the range of operating conditions simulated.

Figure 10 presents a parity plot of the model for hydrodesulfurization reactions for catalysts A and B studied in the present work. The plot between the experimental and simulated sulfur contents in the product appears to be a straight line with a slope close to 1.0, indicating good agreement between the model output and the experimental measurements. The correlation coefficient for the simulation of the hydrodesulfurization reaction is 0.997.

The model can be applied to simulate the performance of the pilot-plant reactor at different operating conditions for which experimental data are not available. The model was used to simulate the effects of hydrogen sulfide and operating pressure on hydrodesulfurization. Figure 11 shows the variation of the product sulfur content with the volume fraction of hydrogen sulfide in

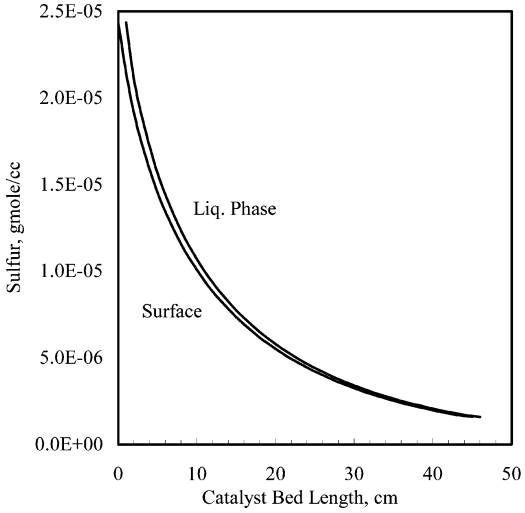

Figure 3. Sulfur concentration along the catalyst bed length in the pilot-plant trickle-bed reactor.

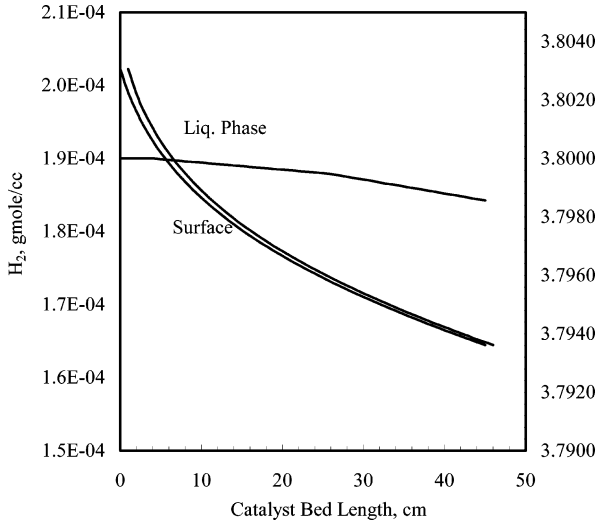

Figure 4. H_2 concentration and partial pressure along the catalyst bed length in the pilot-plant trickle-bed reactor.

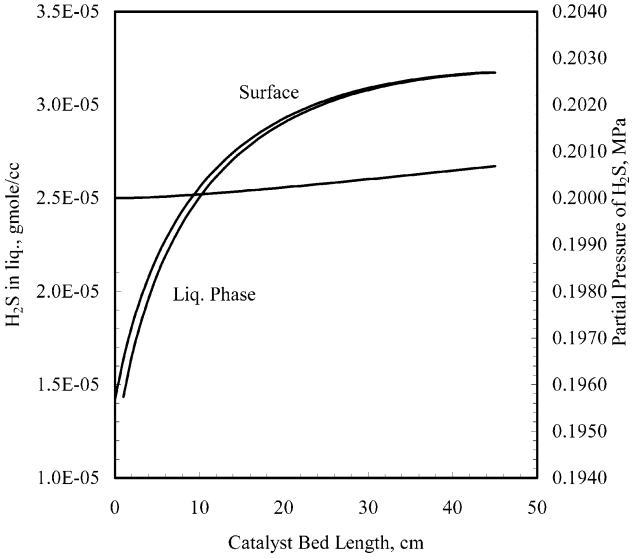

Figure 5. H_2S concentration and partial pressure along the catalyst bed length in the pilot-plant trickle-bed reactor.

Table 4. Simulation of the Pilot-Plant Trickle-Bed Reactor vs Experimental Data with Catalyst A: Effect of Operating Conditions on Product Sulfur Content and Conversion[a]

		experimental		simulated		
T_R, °C	LHSV, h^{-1}	sulfur, wt %	conversion, wt %	sulfur, wt %	conversion, wt %	deviation, %
320	1.0	0.0895	92.88	0.0982	91.15	−9.72
320	1.5	0.1497	86.51	0.1494	86.54	0.20
320	2.0	0.2020	81.80	0.1910	82.79	5.45
320	2.5	0.2330	79.00	0.2258	79.66	3.09
340	1.0	0.0440	96.04	0.0463	95.83	−5.23
340	1.5	0.0880	92.07	0.0830	92.52	5.68
340	2.0	0.1248	88.76	0.1160	89.55	7.05
340	2.5	0.1513	86.37	0.1451	86.93	4.10
360	1.0	0.0202	98.18	0.0201	98.19	0.50
360	1.5	0.0426	96.16	0.0404	96.36	5.16
360	2.0	0.0637	94.26	0.0635	94.28	0.31
360	2.5	0.0825	93.28	0.0857	92.28	−3.88

[a] Operating pressurure = 4.0 MPa, H_2/oil ratio = 200 L/L.

Table 5. Simulation of the Pilot-Plant Trickle-Bed Reactor vs Experimental Data with Catalyst B: Effect of Operating Conditions on Product Sulfur Content and Conversion[a]

		experimental		simulated		
T_R, °C	LHSV, h^{-1}	sulfur, wt %	conversion, wt %	sulfur, wt %	conversion, wt %	deviation, %
320	1.0	0.0785	93.59	0.0855	92.30	−8.92
320	1.5	0.1347	87.86	0.1339	87.94	0.59
320	2.0	0.1820	83.60	0.1739	84.33	4.45
320	2.5	0.2100	81.08	0.2076	81.30	1.14
340	1.0	0.0395	96.44	0.0398	96.41	−0.76
340	1.5	0.0792	92.86	0.0738	93.35	6.82
340	2.0	0.1124	89.87	0.1051	90.53	6.49
340	2.5	0.1362	87.73	0.1330	88.02	2.35
360	1.0	0.0182	98.36	0.0179	98.39	1.65
360	1.5	0.0384	96.54	0.0358	96.77	6.77
360	2.0	0.0574	94.83	0.0576	94.81	−0.35
360	2.5	0.0745	93.95	0.0787	92.91	−5.64

[a] Operating pressurure = 4.0 MPa, H_2/oil ratio = 200 L/L.

the inlet hydrogen gas. The volume fraction of hydrogen sulfide in the feed gas has a strong effect on the product sulfur content, as hydrogen sulfide inhibits the reaction by adsorbing on active sites. Figure 12 presents the variation of the product sulfur content with the reactor

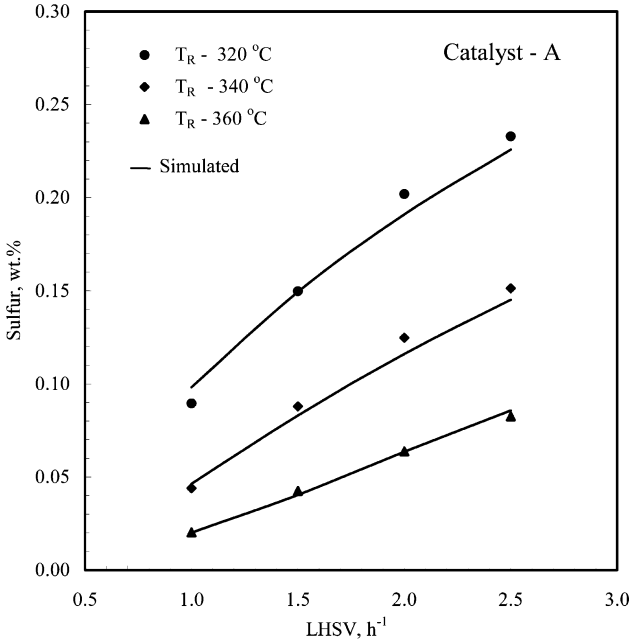

Figure 6. Simulation of the pilot-plant trickle-bed reactor: Effect of liquid hourly space velocity on the product sulfur content.

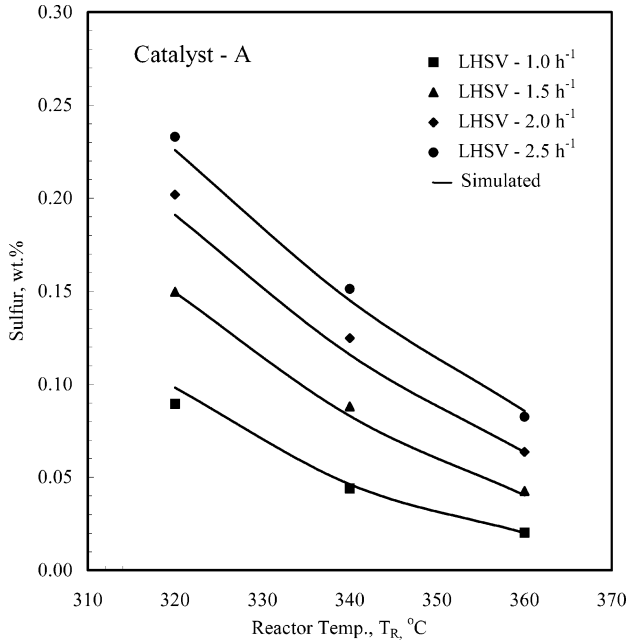

Figure 7. Simulation of the pilot-plant trickle-bed reactor: Effect of reactor temperature on the product sulfur content.

pressure. The product sulfur content was found to decrease with increasing pressure. At higher operating pressure, the concentration of hydrogen in the diesel oil increases because of the increased solubility of hydrogen.

Table 6 reports the effects of reactor temperature on the hydrogenation of aromatics and compares the simulation results with experimental measurements. The model output was found to agree well with the experimental data for the catalysts studied in the present work. The conversion of polyaromatics was found to reach a maximum at a reactor temperature of 340 °C.

The conversion of aromatics is governed by the dynamic equilibrium constants as determined using the van't Hoff correlation. The effect of reactor temperature

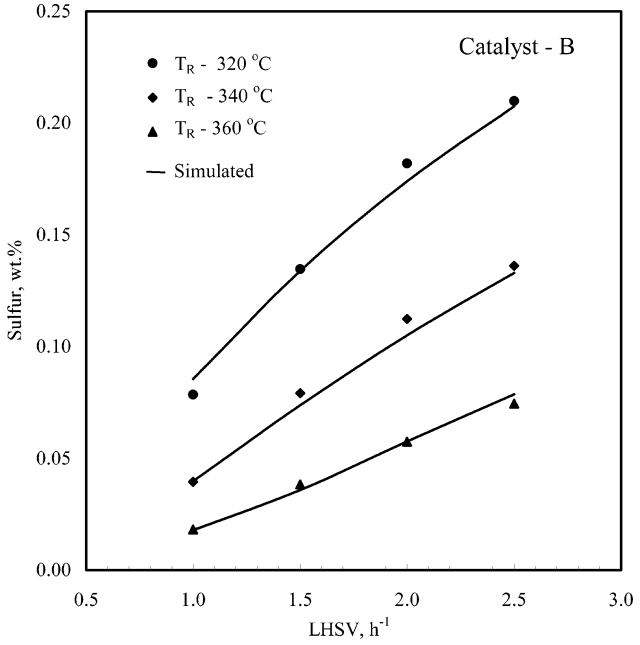

Figure 8. Simulation of the pilot-plant trickle-bed reactor: Effect of liquid hourly space velocity on the product sulfur content.

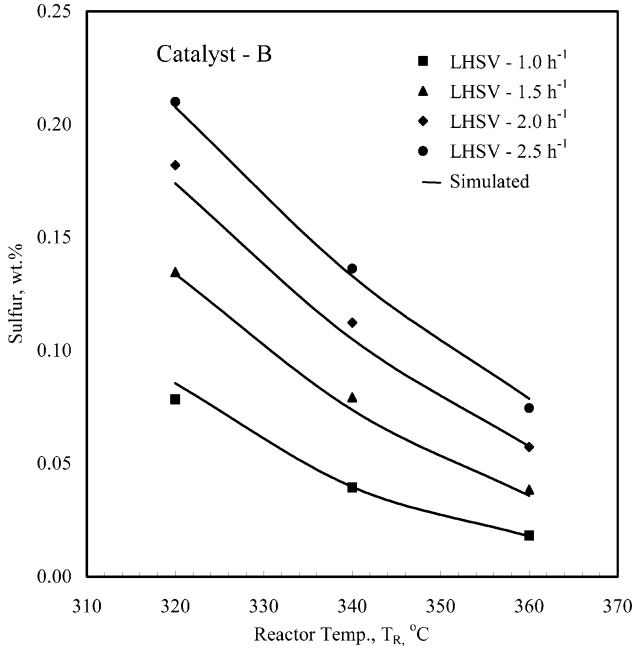

Figure 9. Simulation of the pilot-plant trickle-bed reactor: Effect of reactor temperature on the product sulfur content.

on the thermodynamic equilibrium constants for the hydrogenations of poly-, di-, and monoaromatics is presented in Figure 13. The equilibrium constants are plotted on a logarithmic scale against the absolute reactor temperature. The equilibrium constants decrease with increasing reactor temperature. At higher reactor temperatures, the order of the equilibrium constants is $K_{Poly} > K_{Di} > K_{Mono}$, in contrast to their ranking at lower reactor temperatures, that is, $K_{Mono} > K_{Di} > K_{Poly}$. Similar trends have also been reported by Girgis and Gates,[14] Stanislaus and Cooper,[17] and Chowdhury et al.[12]

The effect of the liquid hourly space velocity on the hydrogenations of poly-, di-, and total aromatics at a reactor temperature of 340 °C is presented in Figure 14. The variations of the conversion of total aromatics,

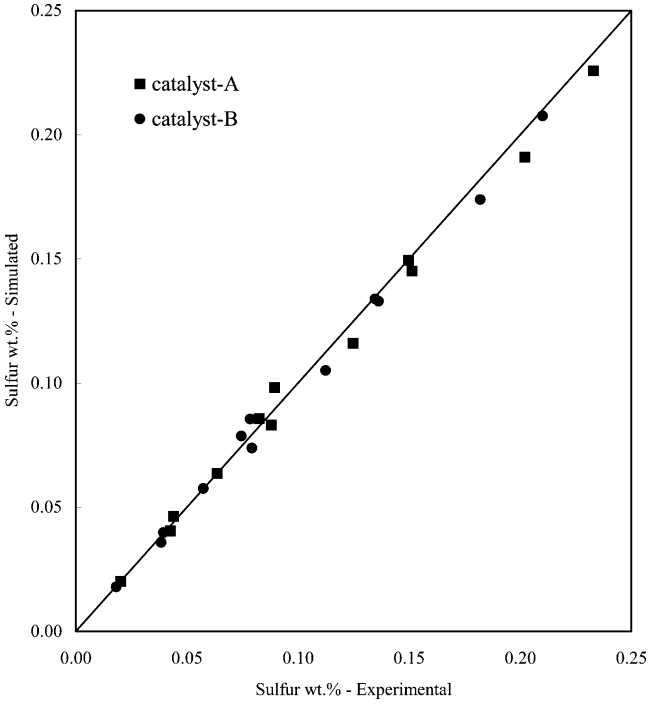

Figure 10. Parity plot of partial wetting model for pilot-plant trickle-bed reactor: Hydrodesulfurization reactions.

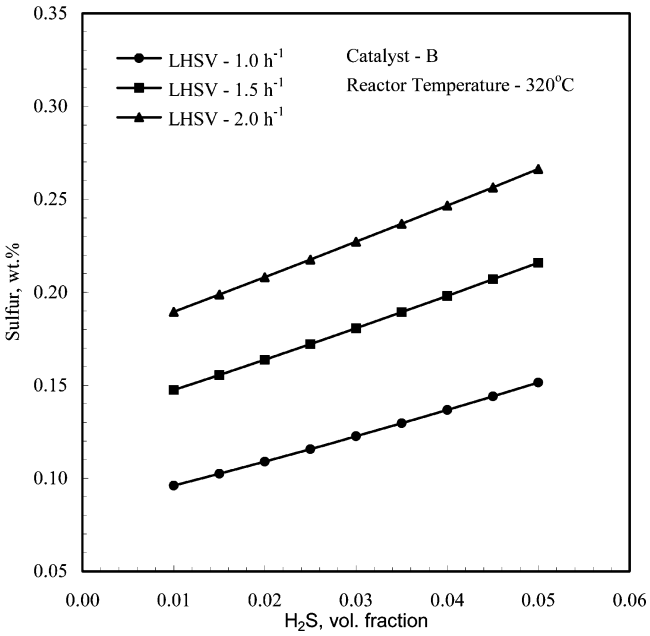

Figure 11. Simulation of the pilot-plant reactor: Effect of H_2S inhibition.

simulated and experimental, with reactor temperature at a constant operating pressure of 4.0 MPa, an LHSV of 2.0 h^{-1}, and a H_2/oil ratio of 200 L/L along with the equilibrium conversions are presented in Figure 15. Similarly, the experimental and simulated effects of reactor temperature, at a constant LHSV of 2.0 h^{-1}, on the conversions of poly-, di-, and monoaromatics along with the equilibrium conversions are shown in Figures 16−18. Negative conversions for di- and monoaromatics are physically justifiable because they depend on the rates at which the reactions from poly- to diaromatics, from di- to monoaromatics, and from monoaromatics to naphthenes proceed. However, the negative conversions for total and polyaromatics shown in Figures 15 and 16

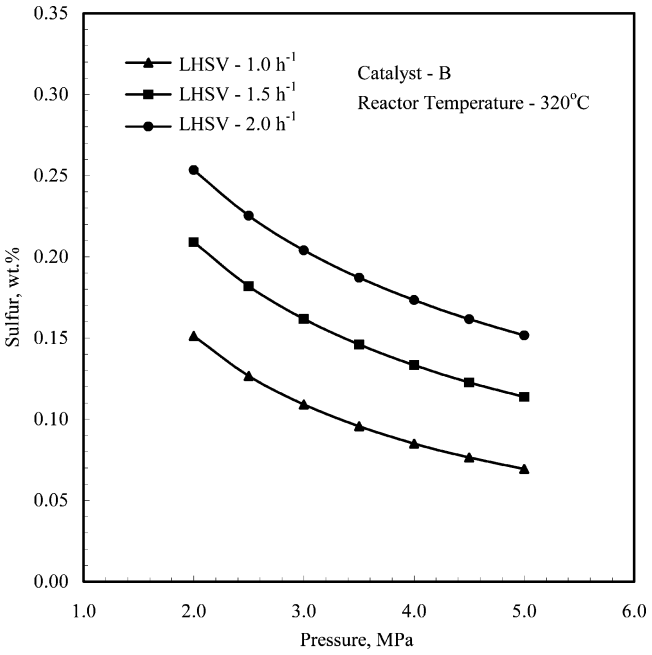

Figure 12. Simulation of the pilot-plant reactor: Effect of pressure.

Table 6. Simulation of the Pilot-Plant Trickle-Bed Reactor vs Experimental Data: Effect of Reactor Temperature on Hydrogenation of Aromatics[a]

concentration in the product, wt %	experimental			simulated		
	320 °C	340 °C	360 °C	320 °C	340 °C	360 °C
			Catalyst A			
polyaromatics	1.3	1.1	2.5	1.20	1.12	2.47
diaromatics	6.3	6.5	10.9	6.27	6.52	10.88
monoaromatics	26.5	26.2	23.8	26.25	26.17	23.76
naphthenes	19.5	19.5	19.3	19.49	19.52	19.25
			Catalyst B			
polyaromatics	1.1	1.0	2.5	1.11	1.07	2.47
diaromatics	5.9	6.2	10.9	5.90	6.33	10.87
monoaromatics	26.5	26.2	23.7	26.44	26.24	23.76
naphthenes	19.4	19.5	19.2	19.52	19.53	19.25

[a] Liquid hourly space velocity = 2.0 h^{-1}, pressure = 4.0 MPa, H_2/oil ratio = 200 L/L.

are only simulated values and do not have physical significance.

The conversion of polyaromatics was higher than those of di- and monoaromatics. At a constant liquid hourly space velocity, the conversion was found to increase up to a reactor temperature of 340 °C and then decrease. This can be explained by the fact that, at higher temperatures, equilibrium is approached, and the reverse reaction becomes as fast as the forward reaction. The overall conversion of monoaromatics was found to be negative up to a reactor temperature of 360 °C. This can be attributed to higher rate of diaromatics hydrogenation, producing monoaromatics, compared to the rate of monoaromatics hydrogenation. The conversion of monoaromatics was found to be more difficult under the operating conditions studied in the present work. As can be seen from Figures 15−18, the actual conversions were found to be lower than the equilibrium conversions.

The model predicts negative conversions for poly- and diaromatics beyond a reactor temperature of 380 °C. The negative experimental point for diaromatics conversion at a reactor temperature of 360 °C is in agreement with

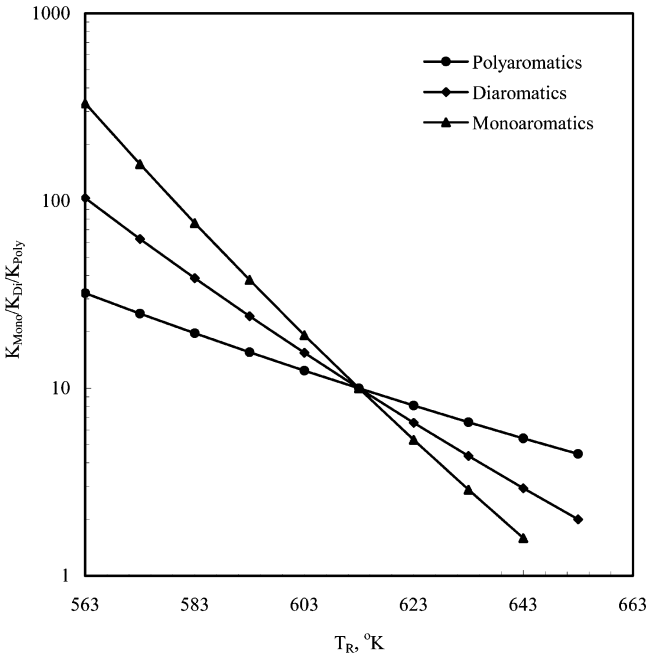

Figure 13. Equilibrium constants for the hydrogenation of mono-, di-, and polyaromatics vs reactor temperature.

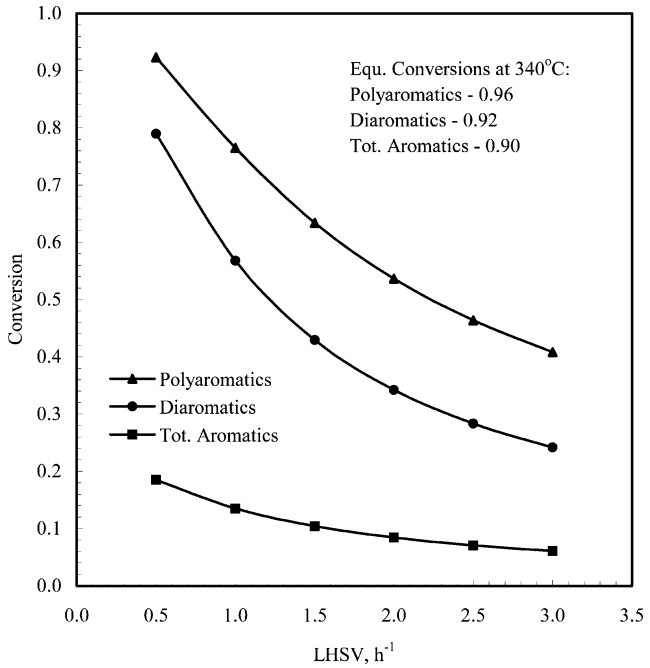

Figure 14. Simulated effect of LHSV on hydrogenation of aromatics.

the model prediction. Cooper at al.[18] and Chowdhury et al.[12] have reported negative conversions for di- and monoaromatics. From the overall analysis of Figures 15−18, the simulated results agree well with the experimental measurements for the hydrodearomatization reactions, as indicated by a correlation coefficient of 0.997.

The model was also applied to simulate the performance of the pilot-plant reactor for the mild hydrocracking and olefin saturation reactions. The yields of light hydrocarbons and wild naphtha were found to increase with increasing reactor temperature. The simulation results for mild hydrocracking and olefin saturation agreed well with the experimental data.

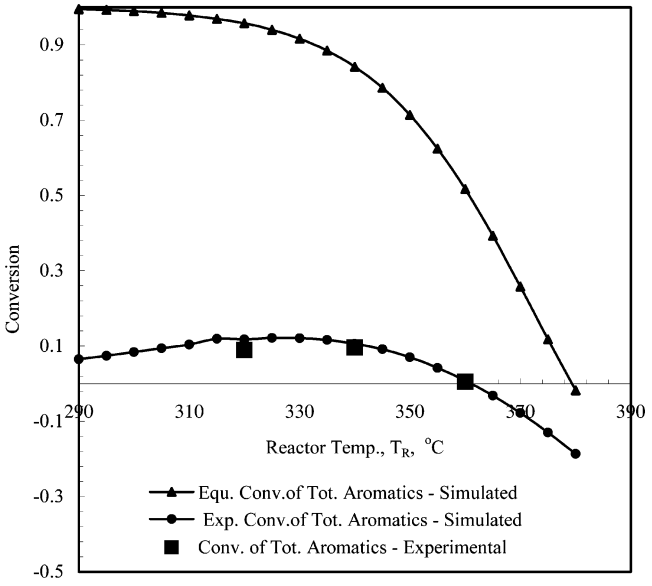

Figure 15. Effect of reactor temperature on total aromatics conversion: Experimental vs simulated.

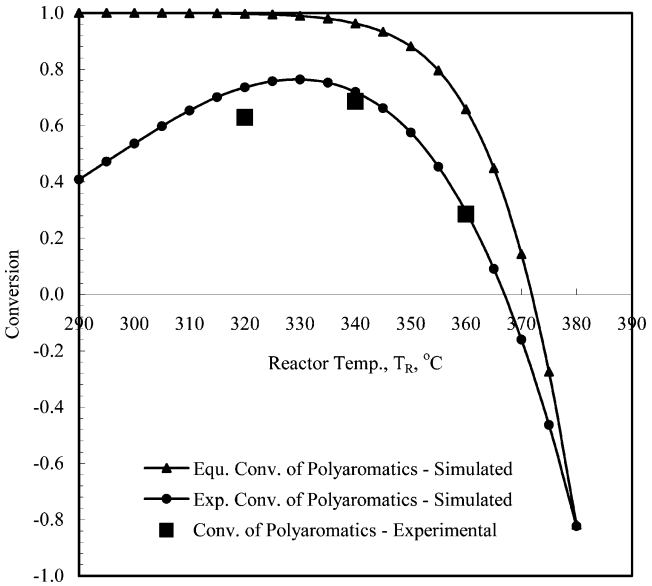

Figure 16. Effect of reactor temperature on polyaromatics conversion: Experimental vs simulated.

Simulation of Industrial Reactors. The industrial reactor unit modeled and simulated in the present work is depicted in Figure 19. The unit is designed to reduce the sulfur content from 1.9 to 0.05 wt % and has two reactors operating in series. The first reactor was loaded with 80 m^3 of catalyst A in three beds with intermittent hydrogen quenching. The diameter of the first reactor is 3.8 m. The second reactor was loaded with 135 m^3 of catalyst B in a single bed with hydrogen quenching at the reactor inlet. The diameter of the second reactor is 4.1 m.

The three-phase nonisothermal reactor model was used to simulate the performance of the industrial reactor. The model solution for the industrial reactor becomes an intial-value problem because the concentrations of reactants and products are known at the reactor inlet. The model was solved with the rate constants estimated from the pilot-plant studies. The wetting efficiency of the catalyst was assumed to be 1.0 considering the high liquid velocities encountered in the industrial reactor.[7,16]

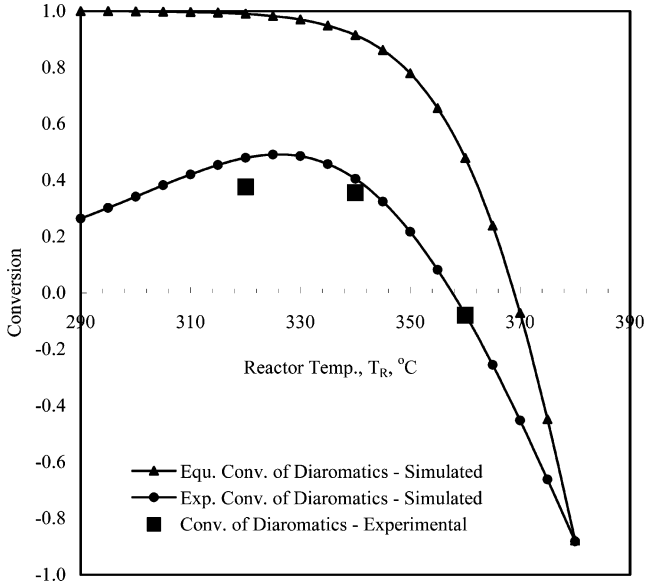

Figure 17. Effect of reactor temperature on diaromatics conversion: Experimental vs simulated.

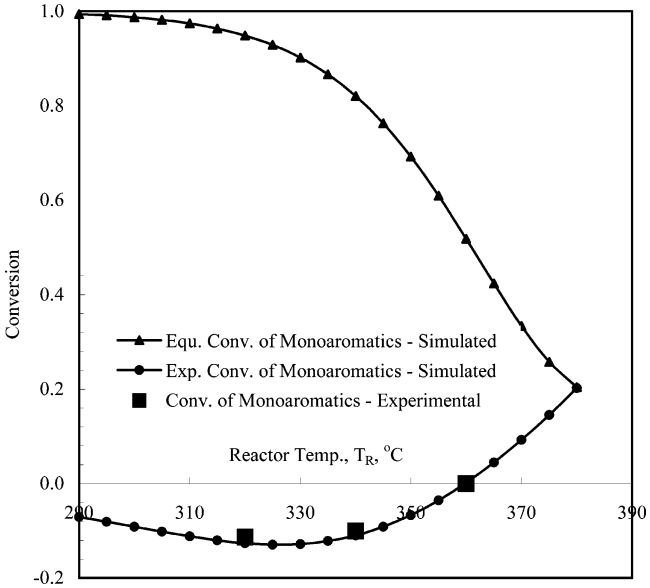

Figure 18. Effect of reactor temperature on monoaromatics conversion: Experimental vs simulated.

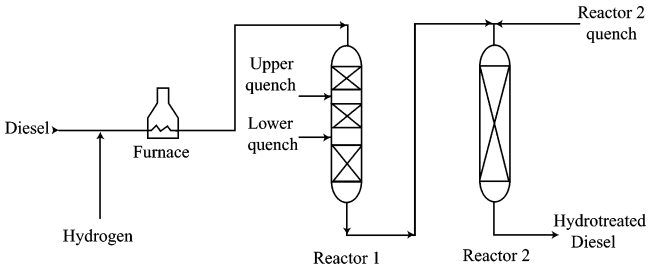

Figure 19. Schematic diagram of industrial trickle-bed reactor system.

Table 7 presents the mass-transfer characteristics of the hydrodesulfrization reaction in trickle-bed reactors. As can be seen from Table 7, the gas and liquid velocities in the pilot-plant reactor are much lower than those in the industrial reactor under normal operating conditions. The higher gas and liquid velocities encountered

Table 7. Mass Transfer in Trickle-Bed Reactors for the Hydrodesulfurization Reaction

	pilot plant	industrial reactor
pressure, MPa	4.0	4.4
reactor temperature, °C	320	320
liquid hourly space velocity, h^{-1}	2.0	3.0
H_2/HC ratio, L/L	200	160
mass velocity of liquid, G_L, g/cm^2•s	0.02	0.51
reactor diameter, cm	2.54	380
catalyst bed length, cm	40	800
superficial liquid velocity, u_L, cm/s	2.8×10^{-2}	0.60
superficial gas velocity, u_G, cm/s	0.24	3.60
diffusivity, cm^2/s		
sulfur compounds, D_S^l	3.96×10^{-4}	
H_2, $D_{H_2}^l$	6.70×10^{-4}	
H_2S, $D_{H_2S}^l$	5.56×10^{-4}	
gas−liquid mass transfer, s^{-1}		
H_2, $k_{H_2}^l a_l$	2.85×10^{-5}	1.11×10^{-4}
H_2S, $k_{H_2S}^l a_l$	2.16×10^{-5}	8.42×10^{-5}
liquid−soild mass transfer, s^{-1}		
S, $k_S^s a_s$	0.18	0.99
H_2, $k_{H_2}^s a_s$	0.26	1.42
H_2S, $k_{H_2S}^s a_s$	0.23	1.25

Table 8. Simulation of Industrial Reactors: Model Prediction vs Operating Data

parameter	industrial reactor operating point	model prediction	deviation, %
reactor pressure, MPa	4.4	4.4	−
H_2/oil ratio	160	160	−
feed rate, m^3/h	270	270	−
reactor temperature, °C	340	340	−
concetration in the reactor outlet:			
sulfur, wt %	0.0145	0.0156	−7.58
nitrogen, ppmw	38	42	−10.53
olefins, wt %	3.0	3.01	−0.33
polyaromatics, wt %	1.1	1.01	8.18
diaromatics, wt %	6.0	6.22	−3.66
monoaromatics, wt %	26.6	26.56	0.15
naphthenes, wt %	19.5	19.29	0.15
wild naphtha, wt %	0.9	0.85	5.55
light hydrocarbons, wt %	0.1	0.11	−10.00

in industrial trickle-bed reactors result in better mass-transfer characteristics compared to those in pilot-plant reactors, which, in turn, result in higher conversions.

The simulation of the industrial reactor with catalysts A and B in the first and second reactors, respectively, along with the actual data collected from the industrial unit and analysis of the product sample are shown in Table 8. The model predictions were found to match closely with the industrial operating point. The model assumptions and parameters satisfactorily represented the performance of the industrial reactor.

The model can also be applied to simulate the performance of the industrial unit at various operating conditions. Figure 20 shows the simulated effect of the feed rate, at different reactor temperatures, on the product sulfur content of the industrial unit with catalysts A and B in the first and second reactors, respectively. As can be seen from Figure 20, the effect of the feed rate is more pronounced at lower reactor temperatures. The effect of the reactor temperature on the product sulfur concentration of the industrial unit with catalysts A and B in the first and second reactors, respectively, is shown in Figure 21. The product sulfur concentration was found to decrease with increasing reactor temperature at a given feed rate. Figures 20 and 21 also include the industrial reactor operating point obtained from the analysis of industrial reactor samples. The industrial reactor operating point was found to be close to the simulated line, indicating good conformity of the model with the operating data.

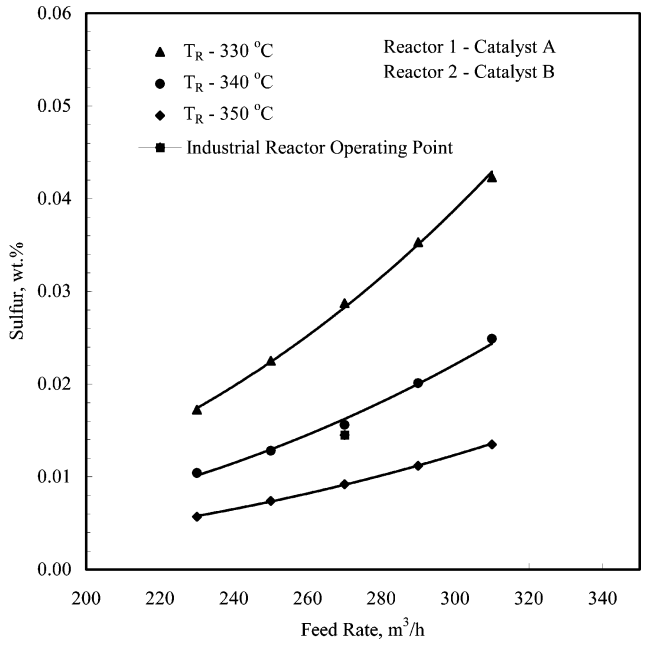

Figure 20. Simulation of industrial trickle-bed reactor: Effect of feed rate on product sulfur.

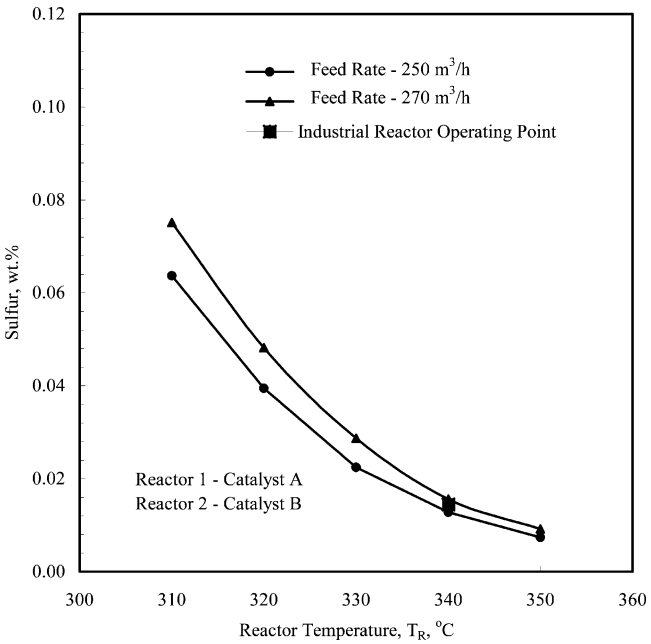

Figure 21. Simulation of industrial trickle-bed reactor: Effect of reactor temperature on product sulfur.

Figure 22 presents the simulation of the temperature along the length of the catalyst beds in both of the reactors and compares these results with the actual temperatures observed in the industrial reactor. The temperature was found to increase by 9, 6, and 10 °C in the first, second, and third beds, respectively, of the first reactor. The temperature was found to increase by 15 °C in the second reactor. The temperature profiles generated using the model were found to reflect actual temperature profiles encountered in industrial reactor.

Conclusions

A three-phase heterogeneous model was developed to describe the performance of pilot-plant and industrial

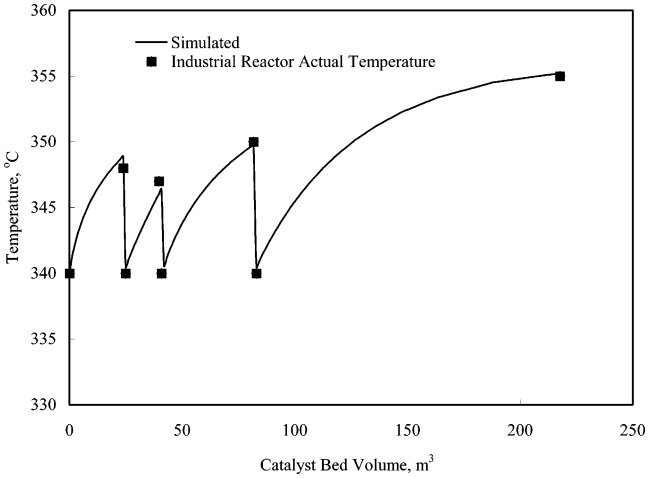

Figure 22. Temperature profile of industrial trickle-bed reactor system: Simulated vs actual.

trickle-bed reactors. Experiments were carried out in a pilot-plant trickle-bed reactor to evaluate two different catalysts for application to diesel hydrodesulfurization. The data generated in the pilot-plant reactor were used to estimate kinetic parameters for various hydrotreating reactions. The model developed in the present work was applied to simulate the performance of the pilot-plant reactor over a wide range of operating conditions. The simulation results were found to agree well with the experimental data. The model was also applied to simulate the performance of an industrial reactor. The model was tested with the data collected from an industrial unit and found to represent its performance adequately. The model was applied to study the influence of the feed rate and reactor temperature on hydrotreating reactions.

Nomenclature

a_p = gas−liquid interfacial area, cm^2
a_s = specific surface area of the catalyst, cm^{-1}
C = concentration, mol/cm^3
C_p = specific heat of the liquid phase, cal/g·K
d_p = diameter of a catalyst particle, cm
H = Henry's coefficient, $MPa·cm^3/mol$
k = rate constant, mol/cm·s
K = dynamic equilibrium constant
k_{ad} = adsorption equilibrium constant for hydrogen sulfide, cm^3/mol
$k_{app,S}$ = apparent rate constant for the desulfurization reaction, $(cm^3/g·s)·(cm^3/mol)^{0.45}$
$K_{in,S}$ = intrinsic rate constant for the desulfurization reaction, $(cm^3/g·s)·(cm^3/mol)^{0.45}$
k_{app} = apparent rate constant, $cm^3/g·s$
k_{in} = intrinsic rate constant, $cm^3/g·s$
k^l = gas−liquid mass-transfer coefficient, cm/s
k^s = liquid−solid mass-transfer coefficient, cm/s
L_b = minimum catalyst bed length, cm
LHSV = liquid hourly space velocity, h^{-1}
m_1 = order of desulfurization reaction with respect to sulfur-containing compounds
m_2 = order of desulfurization reaction with respect to hydrogen
P = reactor pressure, MPa
r = rate of reaction, mol/g·s
R−CH=CH_2 = olefin
R−H = hydrocarbon
R−N = hydrocarbon containing nitrogen
R−S = hydrocarbon containing sulfur
T, T_R = reactor temperatue, °C or K
u = superficial velocity, cm/s
w = weight fraction
z = axial coordinate along the catalyst bed length, cm

Subscripts

p = reactor outlet or product
e = equilibrium
Di = diaromatics
G = gas
H_2 = hydrogen
H_2S = hydrogen sulfide
HC = light hydrocarbons (C_1−C_4 gases)
L = liquid
Mono = monoaromatics
N = nitrogen
Naph = naphthenes
O = olefins
Poly = polyaromatics
S = sulfur
Tot = total aromatics
NH_3 = ammonia
H_2O = water
GO = gas oil or diesel
WN = wild naphtha
0 = reactor inlet or initial conditions

Superscripts

l = liquid
s = catalyst surface

Greek Symbols

ΔH = heat of reaction, cal/mol
ρ = density, g/cm^3
ρ_B = bulk density of catalyst particles, g/cm^3
ξ = fractional catalyst bed dilution
V_c = volume of catalyst particles, cm^3
V_i = volume of inert particles, cm^3
η = catalyst effectiveness factor

Literature Cited

(1) Specchia, V.; Baldi, G. Pressure Drop and Liquid Holdup for Two Phase Concurrent Flow in Packed Beds. *Chem. Eng. Sci.* **1977**, *32*, 515−523.

(2) Al-Dahhan, M. H.; Dudukovic, M. P. Pressure Drop and Liquid Holdup in High-Pressure Trickle-Bed Reactors. *Chem. Eng. Sci.* **1994**, *49*, 5681−5698.

(3) Henry, C. H.; Gilbert, J. B. Scaleup of Pilot Plant Data for Catalytic Hydroprocessing. *Ind. Eng. Process Des. Dev.* **1973**, *12* (3), 328−333.

(4) Iannibello, A.; Marengo, S.; Burgio, G.; Baldi, G.; Sicardi, S.; Specchia, V. Modeling the Hydrotreating Reactions of a Heavy Residual Oil in a Pilot Trickle Bed Reactor. *Ind. Eng. Process Des. Dev.* **1985**, *24* (3), 531−537.

(5) Tsamatsoulis, D.; Papayannakos, N. Simulation of Nonideal Flow in a Trickle Bed Hydrotreater by Crossflow Model. *Chem. Eng. Sci.* **1995**, *50* (23), 3685−3691.

(6) Froment, G. F.; Depauw, G. A.; Valerie, V. Kinetic Modeling and Reactor Simulation in Hydrodesulfurization of Oil Fractions. *Ind. Eng. Chem. Res.* **1994**, *33*, 2975−2988.

(7) Korsten, H.; Hoffman, U. Three Phase Reactor Model for Hydrotreating in Pilot Trickle Bed Reactors. *AIChE J.* **1996**, *42* (5), 1350−1360.

(8) Ramesh Kumar, V.; Balaraman, K. S.; Ramachandra Rao, V. S.; Ananth, M. S. Performance Study of Certain Commercial Catalysts in Hydrodesulfurization of Diesel Oils. *Pet. Sci. Technol.* **2001**, *19* (9−10), 1029−1038.

(9) Mears, D. E. The role of axial dispersion in trickle-flow laboratory reactors. *Chem. Eng. Sci.* **1971**, *26*, 361−1366.

(10) Bhaskar, M.; Balaraman, K. S. Simulation of a pilot plant trickle bed reactor for hydrodesulfurization of diesel fraction. Presented at Petrotech-2001, 4th International Petroleum Conference and Exhibition, New Delhi, India, Jan 9−12, 2001.

(11) Bhaskar, M.; Valavarasu, G.; Meenakshisundaram, A.; Balaraman, K. S. Application of a three phase heterogeneous model to analyze the performance of a pilot plant trickle bed reactor. *Pet. Sci. Technol.* **2002**, *20* (3−4), 251−268.

(12) Chowdhury, R.; Pedernera, E.; Reimert, R. Trickle Bed Reactor Model for Desulfurization and Dearomatization of Diesel. *AIChE J*. **2002**, *48* (1), 26−135.

(13) Ma, X.; Kinya, S.; Takaaki, I.; Isao, M. Hydrodesulfurization Reactivities of Narrow-Cut Fractions in a Gas Oil. *Ind. Eng. Chem. Res.* **1995**, *34*, 748−754.

(14) Girgis, M. J.; Gates, B. C. Reactivities, Reaction Networks and Kinetics in High-Pressure Catalytic Hydroprocessing. *Ind. Eng. Chem. Res.* **1991**, *30*, 2021.

(15) Willson, M. F.; Kriz, J. F. Upgrading of Middle Distillate Fractions of a Syncrude from Athabasca Oil Sands. *Fuel* **1984**, *63*, 190−196.

(16) Satterfield, C. N. Trickle Bed Reactors. *AIChEJ*. **1975**, *21*, 1.

(17) Stanislaus, A.; Cooper, B. H. Aromatic Hydrogenation Catalysis: A Review. *Catal. Rev. Sci. Eng.* **1994**, *36*, 75.

(18) Cooper, B. H.; Sogaard-Anderson, P.; Nielsen-Hannerup, P. Catalytic Hydroprocessing of Petroleum and Distillates. In *Proceedings of the AIChE Spring National Meeting*; Marcel Dekker: New York, 1993; pp 279−290.

Received for review April 30, 2004
Revised manuscript received July 21, 2004
Accepted August 11, 2004

IE049642B